applied sciences

MDPI

Article

Femtosecond Optical Laser System with Spatiotemporal Stabilization for Pump-Probe Experiments at SACLA

Tadashi Togashi [1,2,*], Shigeki Owada [1,2], Yuya Kubota [2], Keiichi Sueda [2], Tetsuo Katayama [1,2], Hiromitsu Tomizawa [1,2], Toshinori Yabuuchi [1,2], Kensuke Tono [1,2] and Makina Yabashi [1,2]

1 Japan Synchrotron Radiation Research Institute, 1-1-1 Kouto, Sayo-cho, Sayo-gun, Hyogo 679-5198, Japan; osigeki@spring8.or.jp (S.O.); tetsuo@spring8.or.jp (T.K.); hiro@spring8.or.jp (H.T.); tyabuuchi@spring8.or.jp (T.Y.); tono@spring8.or.jp (K.T.); yabashi@spring8.or.jp (M.Y.)

2 RIKEN SPring-8 Center, 1-1-1 Kouto, Sayo-cho, Sayo-gun, Hyogo 679-5148, Japan; kubota@spring8.or.jp (Y.K.); sueda-k@spring8.or.jp (K.S.)

* Correspondence: tadashit@spring8.or.jp

Received: 15 October 2020; Accepted: 6 November 2020; Published: 9 November 2020

Abstract: We constructed a synchronized femtosecond optical laser system with spatiotemporal stabilization for pump-probe experiments at SPring-8 Angstrom Compact Free Electron Laser (SACLA). Stabilization of output power and pointing has been achieved with a small fluctuation level of a few percent by controlling conditions of temperature and air-flow in the optical paths. A feedback system using a balanced optical-microwave phase detector (BOMPD) has been successfully realized to reduce jitter down to 50 fs. We demonstrated the temporal stability with a time-resolved X-ray diffraction measurement and observed the coherent phonon oscillation of the photo-excited Bi without the post-processing using the timing monitor.

Keywords: XFEL; ultrafast laser; pump-probe experiment; timing synchronization

1. Introduction

X-ray free-electron lasers (XFELs) [1–7] have significant impacts on a variety of scientific fields. In particular, coherent X-ray pulses with an ultrafast temporal duration (<10 fs) have enabled observation of the electronic and structural dynamics of matter with an ångström and femtosecond spatiotemporal resolution. Owing to the ultrashort pulses in the X-ray region, remarkable scientific progress has been reported in studies on capturing ultrafast dynamics in light-induced chemical reactions [8–12], phase transition [13–16], coherent phonon oscillation [17], and spin states [18]. These studies had been carried out using pump-probe techniques combined with femtosecond optical lasers; therefore, the stabilities of not only the output power of the lasers but pointing and timing are crucial for the success of experiments. Recently, high-power laser systems based on fiber lasers have been developed for user experiments [19–22] under high repetition rate operation of the megahertz order in the European XFEL [4] and the Linac Coherent Light Source II (LCLS-II) [3]. In XFEL facilities operating at several-tens to a hundred hertz—such as the LCLS [2], SPring-8 Angstrom Compact Free Electron Laser (SACLA) [5], the Pohang Accelerator Laboratory X-ray free-electron laser (PAL-XFEL) [6], and Swiss X-ray Free Electron Laser (SwissFEL) [7]—stabilization techniques adapted to synchronized optical laser systems are keys of precise measurement for pump-probe experiments.

In SACLA, we installed a femtosecond optical laser system and constructed components of amplification, transport, pulse compression, and frequency conversion for time-resolved experiments. The operation of this laser system has been stabilized in terms of power and pointing by controlling conditions of temperature and air-flow in the optical path. Regarding the timing of the laser system,

we had employed a synchronization system with direct detection of an optical pulse train, which has a jitter of ~0.3 ps [23–25]. Recently, a feedback system using a "balanced optical-microwave phase detector (BOMPD)" working at a C-band frequency was developed and enabled reduction of the jitter down to ~50 fs. In this paper, we introduce the optical components of the laser system and the results of the stabilized operation. The femtosecond pulses produced by the laser system are provided for user experiments by time-resolved X-ray absorption and emission spectroscopy, X-ray diffraction, and X-ray scattering.

2. Laser System

The optical laser system has been installed in a thermo-stabilized laser hutch 1 (LH1) next to experimental hutches (EH1 and EH2) of SACLA and provides femtosecond pulses for time-resolved experiments at EH2 and EH4c of Beamline 3 (BL3) [26]. This laser system, which is based on a chirped pulse amplification [27] of a Ti:sapphire laser, comprises a mode-locked oscillator, a pulse stretcher, a regenerative amplifier, a multi-pass amplifier, and pulse compressors (shown in Figures 1 and 2). Optical pulses generated by the oscillator at 79.3 MHz are stretched up to 0.2 ns and amplified to 5 mJ by the regenerative amplifier at 960 Hz (Legend Elite, Coherent Inc., Santa Clara, CA, USA. An "acousto-optic programable dispersive filter (AOPDF)" (Dazzler, FASTLITE, Antibes, France) [28] before the stretcher can compensate and optimize dispersion in the optical path. The output pulses from the regenerative amplifier are divided by a Pockels Cell at the operation frequency of SACLA (60 Hz). Ten percent of these pulses split by a partial reflection mirror is directed to the experimental hutch 1 (EH1) for a timing monitor (described in Section 3). The seven-pass amplifier multiplies the rest of the pulses (90% in pulse energy) to 20 mJ at 60Hz. The amplified main beam with about 4-mm diameter (FWHM, the full width at half maximum) is propagated without pulse compression to EH2 and EH4c. The power ratio between the two beams toward EH2 and EH4c is variable with a half-wave plate and a polarization beam splitter. The three transport lines toward EH1, EH2, and EH4c with distances of 3, 4, 16 m, respectively, are built on the floor of the experimental hall. The mirror holders of the transport lines, designed for long term stability (Polaris, Thorlabs Inc., Newton, NJ, USA), are mounted on massive lead blocks to avoid vibration from the floor. These transport lines, including the optics, are covered with ducts to suppress fluctuation from air-flow.

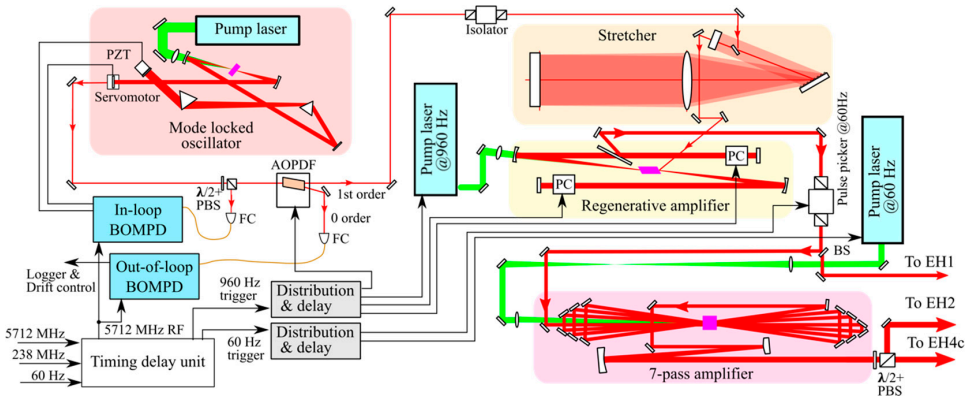

Figure 1. Laser system at LH1. Optical pulses generated by a mode-locked oscillator at 79.3 MHz are stretched up to 0.2 ns and amplified to 5 mJ by a regenerative amplifier at 960 Hz. Output pulses from the regenerative amplifier are picked up at 60 Hz by a Pockels Cell (PC) and multiplied to 20 mJ by a seven-pass amplifier. The amplified pulses without pulse-compression are transported to EH2 and EH4c and compressed in each experimental hutch (Figure 2). 10% of the output of the regenerative amplifier is used for the timing monitor at EH1. The synchronization system using a balanced optical-microwave phase detector (BOMPD) is installed to the oscillator. λ/2+PBS: a half-wave plate and a polarization beam splitter; FC: a fiber coupler; AOPDF: an acousto-optic programable dispersive filter; BS: a 90% partial reflection mirror for beam splitting.

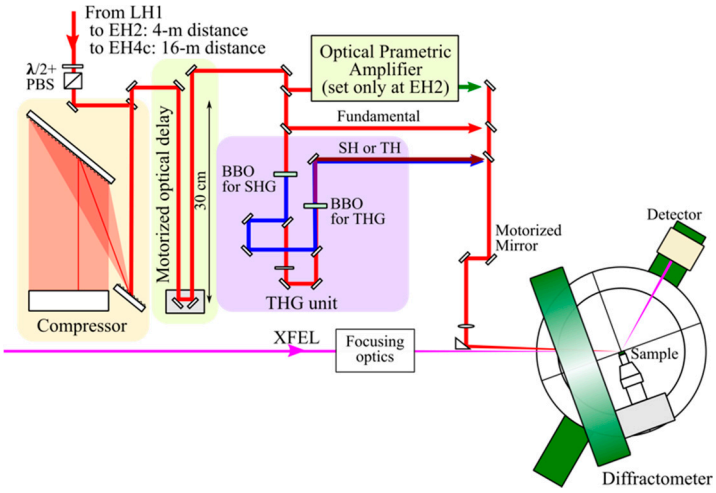

Figure 2. Optical layout at EH2 and EH4c. A compressor, delay line, and THG unit are set up on an optical bench at EH2 and EH4c. An optical parametric amplifier (OPA) is available at EH2. The optical laser beam is focused on a sample with an almost parallel direction to the XFEL beam. Setup for time-resolved X-ray diffraction is indicated as a typical pump-probe experiment.

A compressor, a delay line, and a third-harmonic generation (THG) unit are installed on an optical bench in each of EH2 and EH4c, as shown in Figure 2. Before the grating-pair compressor, the optical beam is expanded to 6 mm in diameter (FWHM) not to damage the gratings. A typical spectrum of the compressed pulses is shown in Figure 3. Finally, ultrashort pulses of 12 mJ with a 40-fs pulse duration are provided for user experiments at EH2 and EH4c. The fluctuation of the output energy is about 4% in 24 h, as shown in Figure 4. A roof mirror on a 30-cm-long motorized stage (HPT-2, Kohzu Precision Co., Kawasaki, Japan) enables users to tune and scan the delay between the optical and the XFEL pulses with a 6.67-fs step in the range of 2 ns. This long stage has been customized to suppress pitching and yawing motion below five arcminutes (~1.5 mrad). Second-harmonic (SH) and third-harmonic (TH)—whose wavelengths are 400 nm and 267 nm, respectively—are generated by the THG unit on users' demand. A type-I β-BaB2O4 (BBO) crystal with 0.1-mm thickness is used for SH generation. A TH beam is generated as a sum-frequency mixing of the SH and the remaining fundamental beams by a 0.5-mm thick type-I BBO crystal. Before the incidence to the BBO crystal for the TH generation, polarization and optical path lengths of the SH and the fundamental beams are tuned by a half wave-plate and a delay line. The maximum energy and pulse duration of the fundamental, SH, and TH pulses are summarized in Table 1. At EH2, an "optical parametric amplifier (OPA)" (TOPAS HE-PRIME, Light Conversion, Vilnius, Lithuania) enables users to use tunable ultrafast pulses in the wavelength range from 0.24 to 2.6 μm. Figure 5 indicates the output energy of OPA as a function of wavelength.

The shapes of the fundamental pulses are optimized by tuning the compressor and the AOPDF parameters, monitored with "Spectral Phase Interferometry for Direct Electric-field Reconstruction (SPIDER)" [29] (Venteon SPIDER, Laser Quantum) in periodic maintenance. Figures 6 and 7 show interferometrical traces measured by SPIDER (Figures 6a and 7a) and reconstructed pulses with a ~40-fs pulse duration (Figures 6b and 7b) at EH2 and EH4c, respectively, after the pulse shape optimization in each hutch. The optimized pulses are available in either of the experimental hutches because the difference in optical path lengths to the hutches makes it difficult to find a common condition for the optimization. We constructed a "frequency-resolved optical gating (FROG)" [30], which captures spectra of nonlinear signals with scanning an optical delay, to characterize the SH and TH pulses in the ultraviolet region. As an inspection of the home-build FROG, we measured the shape of the fundamental pulse with SH generation FROG at EH2, as shown in Figure 8. Although dispersion caused by internal optics in the FROG remains, the reconstructed pulse shape is consistent with the SPIDER measurement. Figures 9 and 10 show the FROG traces measured by the self-diffraction

FROG (Figures 9a and 10a) and reconstructed pulses (Figures 9b and 10b) of SH and TH pulses, respectively. As a result, the pulse durations of ~30 fs and ~50 fs were obtained for the SH and TH generation, respectively.

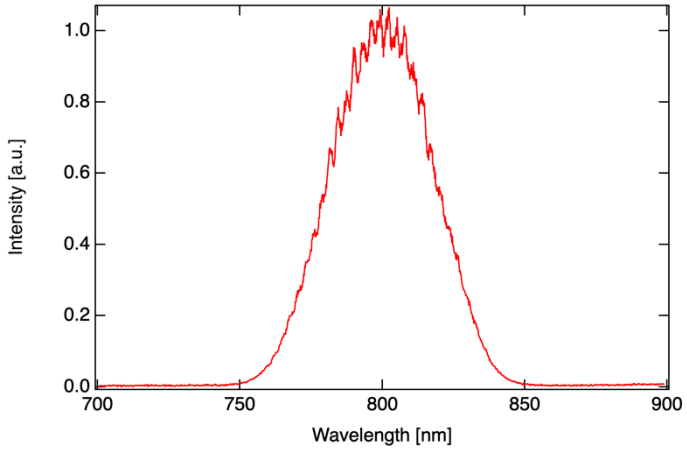

Figure 3. Typical spectrum of the compressed fundamental beam.

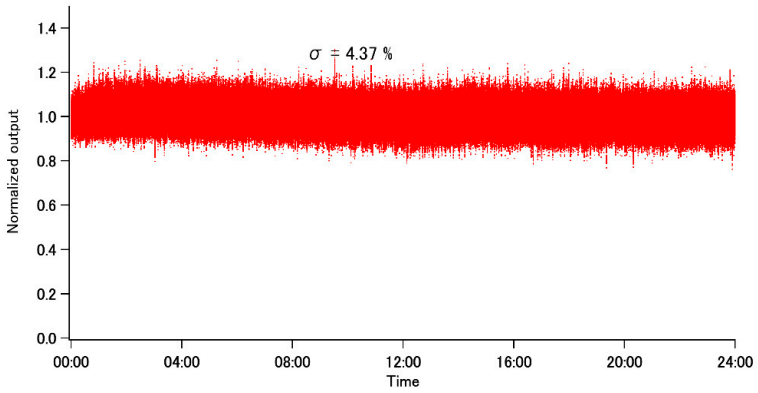

Figure 4. Output trend for 24 h. The vertical axis is normalized with the average.

Table 1. Specification of the fundamental, SH, and TH of the optical laser

	Fundamental	Second Harmonic	Third Harmonic
Wavelength	800 nm	400 nm	267 nm
Pulse energy	~12 mJ	~0.5 mJ	~0.2 mJ
Pulse duration	~40 fs	~30 fs	~50 fs

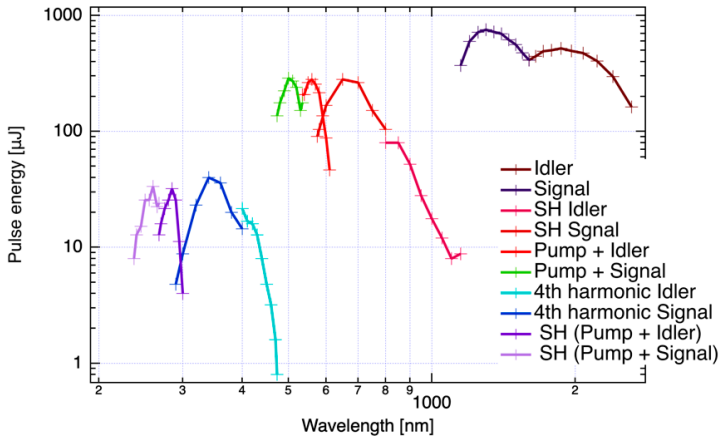

Figure 5. OPA output energy as a function of wavelength in the range from near-infrared to deep ultraviolet.

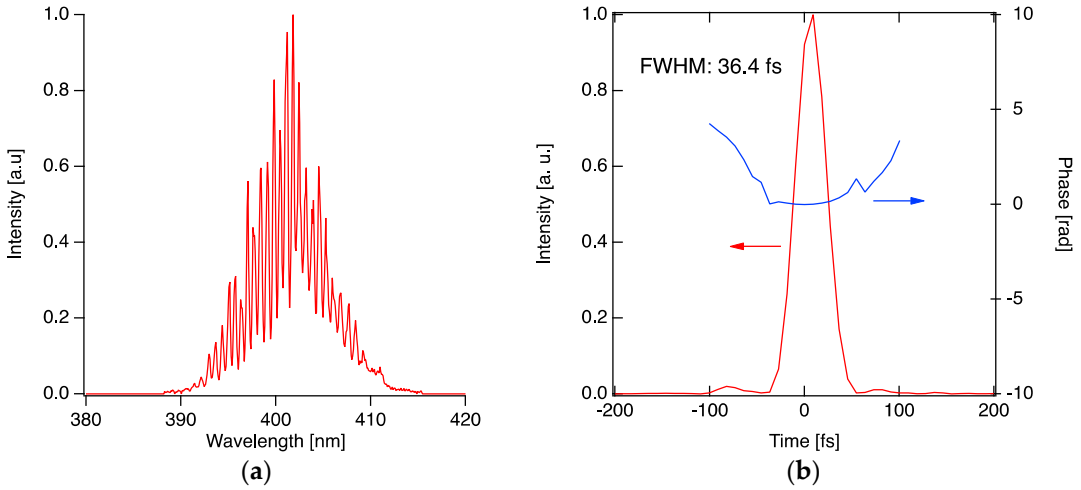

Figure 6. (**a**) SPIDER trace; (**b**) reconstructed intensity (red) and phase (blue) at EH2.

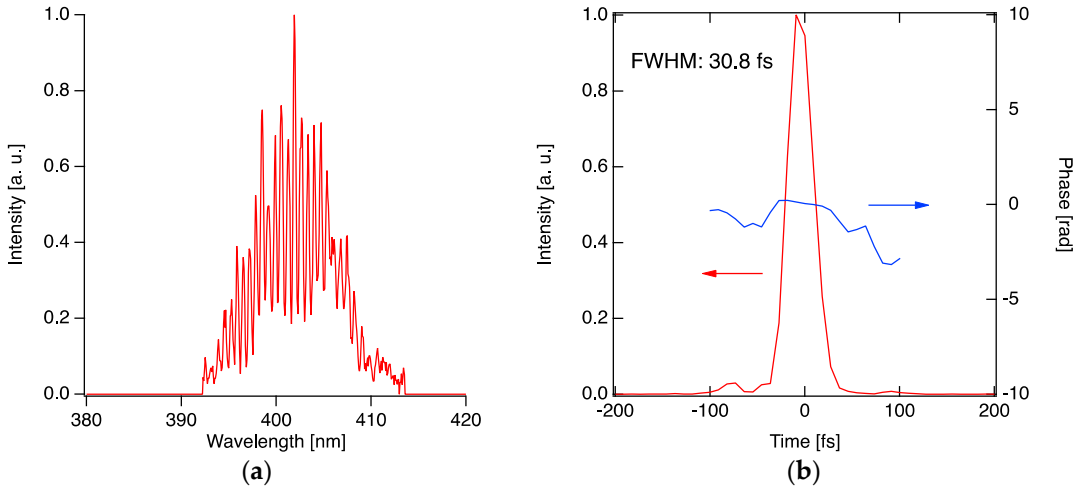

Figure 7. (**a**) SPIDER trace; (**b**) reconstructed intensity (red) and phase (blue) at EH4c.

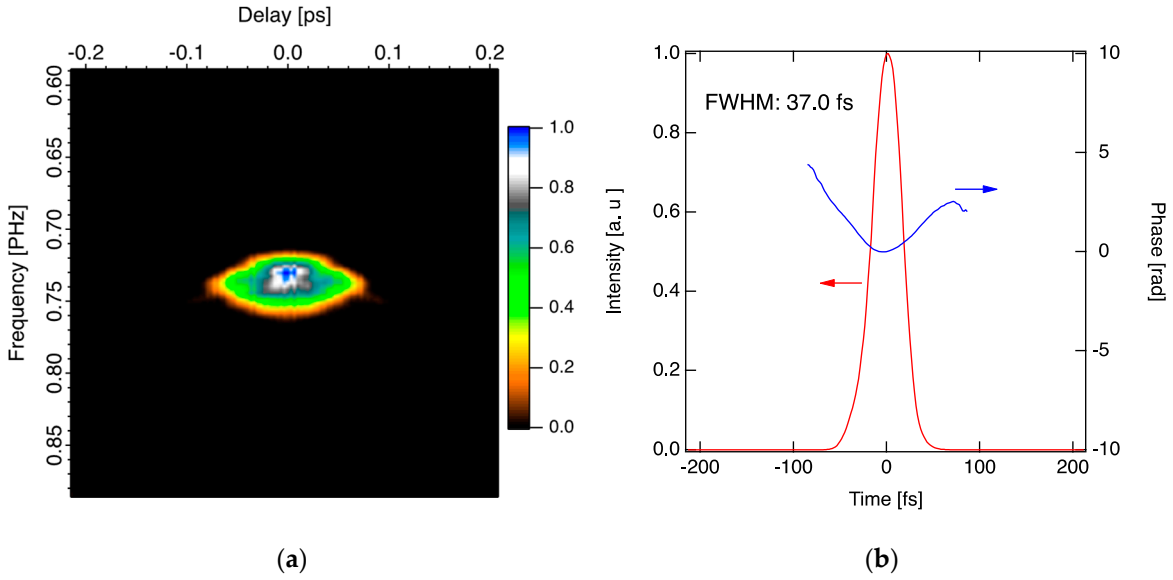

Figure 8. (**a**) FROG image; (**b**) Reconstructed intensity (red) and phase (blue) of the fundamental pulse at EH2.

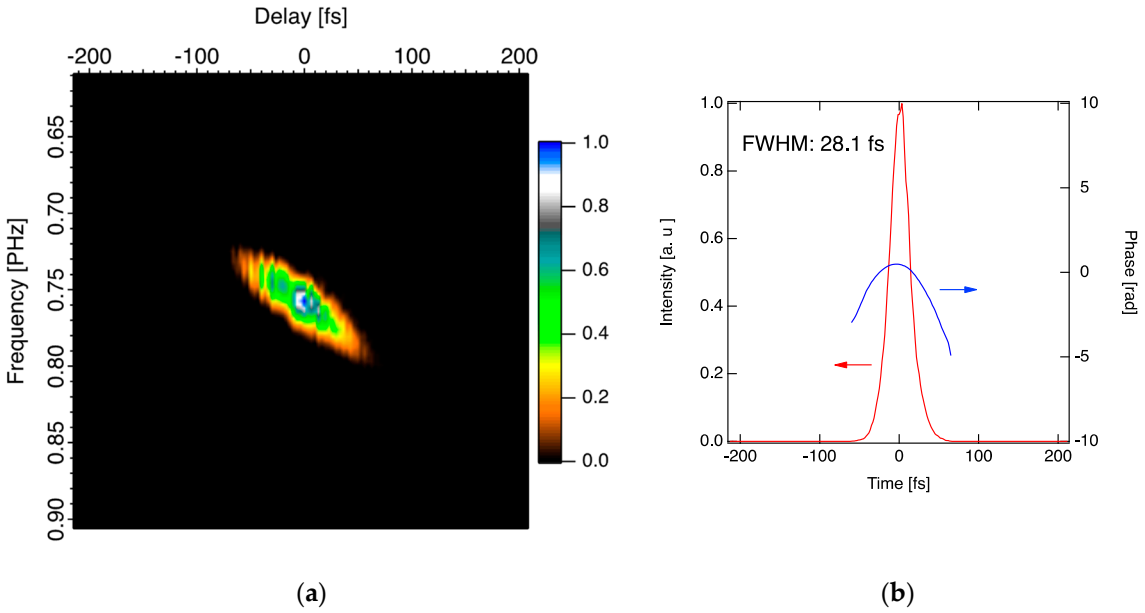

(**a**) (**b**)

Figure 9. (**a**) FROG image; (**b**) reconstructed intensity (red) and phase (blue) of the SH pulse at EH2.

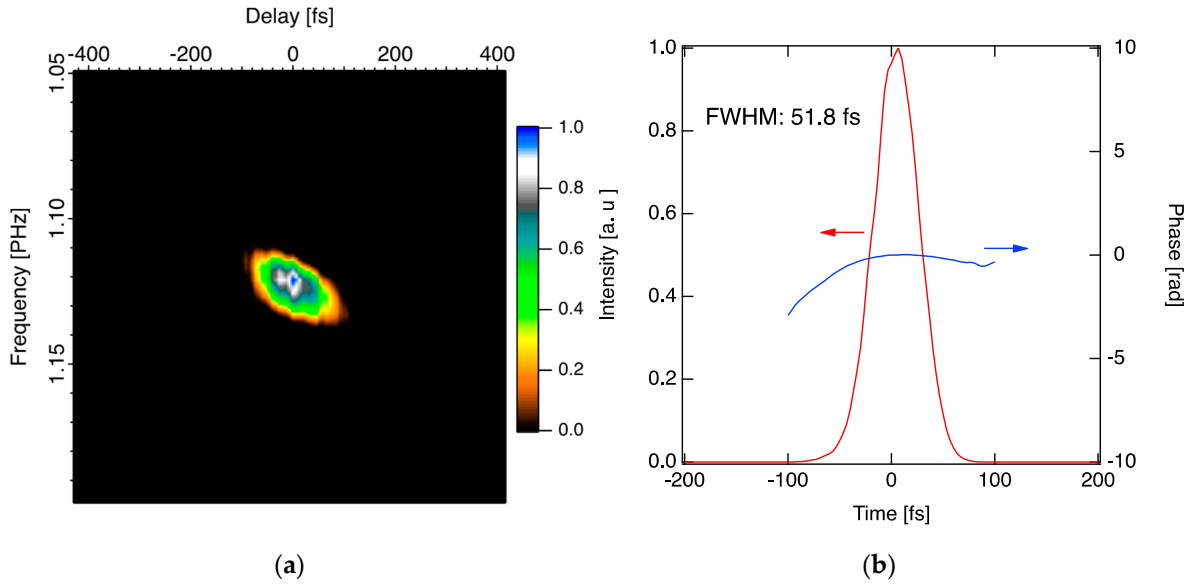

(**a**) (**b**)

Figure 10. (**a**) FROG image; (**b**) reconstructed intensity (red) and phase (blue) of the TH pulse at EH2.

As a typical pump-probe experiment, a time-resolved X-ray diffraction setup is illustrated in Figure 2. The optical laser beam is propagated to a sample almost parallel to the XFEL beam through a prism shape mirror. A typical spot profile focused by a 1-m focal-length lens at the focal position of XFEL in EH2 is indicated in Figure 11a. We evaluated the pointing stability by measuring the centroid position of the beam spot in a shot by shot manner at EH2. Figure 11b shows the trends of the vertical and horizontal positions in 24 h. Although the beam spot drifted by about 10% of the beam size in the warming-up period (the first 4 h), the pointing fluctuations were kept at ~3% (rms). We performed the same measurement at EH4c and obtained almost the same results of the pointing stability.

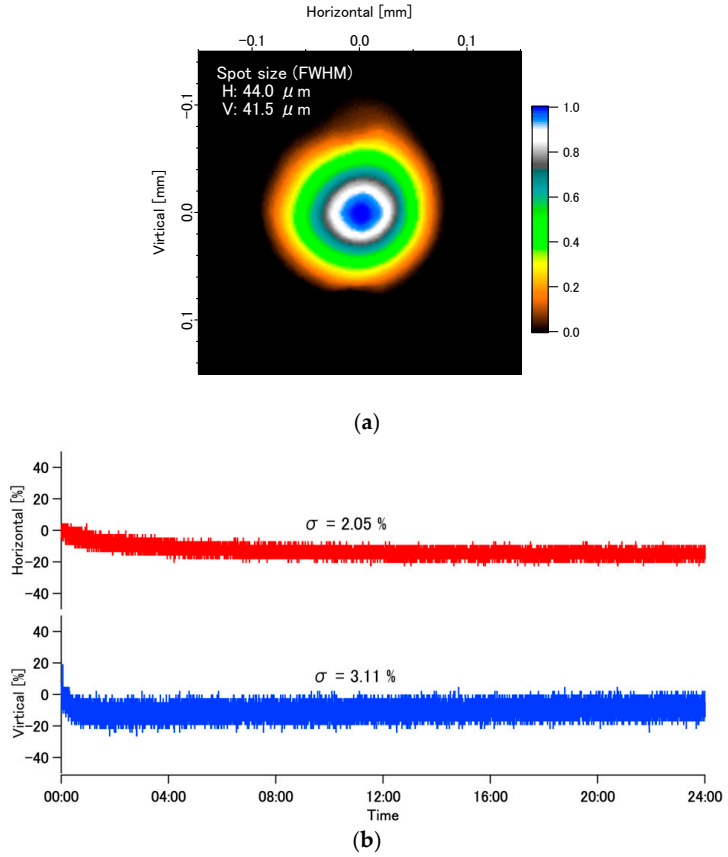

Figure 11. (**a**) Focusing spot profile; (**b**) variety of centroid positions normalized by the beam size (FWHM) in 24 h at EH2.

3. Synchronization of Laser

Precise synchronization to XFEL pulses is realized by controlling the cavity length of the mode-locked oscillator using the 5.7-GHz RF signal for the accelerator operation. The schematic diagram of the control system is shown in the oscillator part of Figure 1. The timing between the pulse train from the oscillator and the RF signal is detected by a BOMPD, which is based on a detecting technique of a phase-error dependent intensity imbalance between two outputs from a "Sagnac-loop" interferometer [31–33]. The repetition rate of the oscillator is locked by applying the phase error signal from 'in-loop' BOMPD (BOMPD-8-SD, Cycle GmbH, Hamburg, Germany) to the linear actuator of the cavity mirror in the mode-locked oscillator. In general, a control system in a feedback loop keeps all the noise sources at the frequencies lower than the locking bandwidth at zero, including the detector's and feedback system's noises and environmental sensitivity. Therefore, an 'out-of-loop' BOMPD (BOMPD-8-MD, Cycle GmbH, Hamburg, Germany) is necessary to characterize the long-term relative phase error between the mode-locked oscillator and the RF signal. The 5.7-GHz RF signal is split and connected with the 'in-loop' and the 'out-of-loop' BOMPDs. About 10% of the oscillator output, which is split by a polarization beam splitter (PBS) and a half waveplate at the oscillator exit, is required as the 'in-loop' BOMPD input for a stable feedback loop. The remaining beam split by the PBS has the almost minimum pulse energy required as a seeder of the regenerative amplifier. Therefore, the zero-order beam of the AOPDF output is used for the 'out-of-loop' BOMPD. The first-order beam diffracted at 960 Hz by the AOPDF is injected into the regenerative amplifier, while the zero-order beam with enough power is delivered to the BOMPD through an optical fiber. We analyzed the phase error, i.e., jitter, from a phase noise spectral density of the 'out-of-loop' BOMPD output measured by a phase noise analyzer (FSWP8, Rohde & Schwarz GmbH & Co. KG, Munich, Germany) with a

calibrated sensitivity of 0.22 mV/fs, as shown in Figure 12. A jitter of 47 fs was achieved by integrating the spectral density from 10^0 to 10^6 Hz.

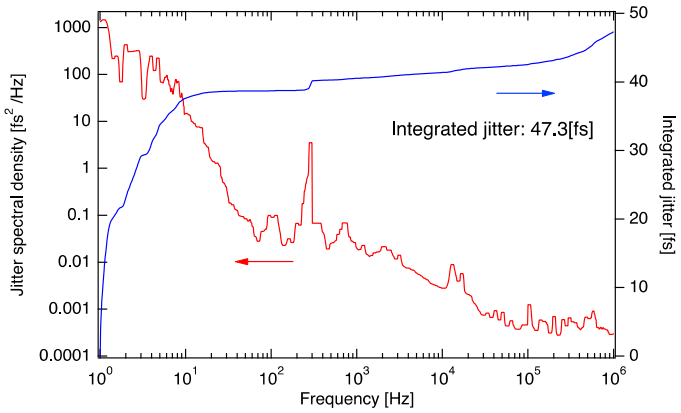

Figure 12. Jitter spectral density (red) measured by a phase noise analyzer (FSWP8, R&S) with a calibrated sensitivity of 0.22 mV/fs and integrated jitter (blue).

Precisely synchronized RF and timing signals of 5712 MHz, 238 MHz, and 60 Hz are provided from the SACLA accelerator to LH1 over several hundred meters through multiple optical fiber delivery systems. The fiber length of this system is feedback-controlled by an interferometer between the going and returning signals. The required signals of 960 Hz and 60 Hz for the laser operation are produced by counting 238-MHz RF and re-clocking with 5712-MHz RF in a timing delay unit (TDU: 86DgR238B01, CANDOX Systems, Gyoda, Japan) [34]. Because the accelerator operation is synchronized to the AC power line for the stabilization of the electron beam, the timing of the electron bunch has a shot-to-shot fluctuation of about 50 µs. The synchronization to the electron bunch is realized by resetting the count of RF with the 60-Hz timing signal reflecting the timing of the electron bunch. The TDU, including counters and in-phase and quadrature (IQ) phase shifters, can delay the 5.7 GHz, 960 Hz, and 60 Hz timing signals for the synchronized laser system simultaneously. The block diagram of the TDU is drawn in Figure 13. Users can change a time interval between the optical laser and the XFEL pulses using the TDU from −2 to +990 microsecond (positive: the XFEL pulses arrives after the optical laser pulses, negative: opposite) with sub-picosecond accuracy.

We have developed a relative arrival timing monitor between the XFEL and the optical laser pulses. The timing monitor, which is based on a spatial decoding method using a transient optical transmittance change of gallium arsenide (GaAs) irradiated by intense X-ray pulses, can sort data sets of pump-probe measurements in the order of the arrival time to correct the error due to the jitter in post-processing [23–25,35,36]. Figure 14 shows the optical setup of the timing monitor at EH1. About 10% of the XFEL beam is split by a transmission grating and vertically focused on the GaAs target in the timing monitor by an elliptical mirror [24]. The horizontal incident angle is set at 45 degrees toward the target normal for the spatial decoding. As described in Section 1, 10% of the optical laser beam before the seven-pass amplifier is transported to EH1 and compressed by a pair of transmission gratings. We installed a linear stage delay line and a 1-m long multi-roundtrip delay line at EH1 to match the optical path length with that to the sample position at EH2 or EH4c. The optical path to the sample position is different according to an experimental hutch in use (EH2 or EH4c), an experimental setup, and a use state of the optical frequency conversion units (SH, TH, and OPA). The optical laser beam propagates along the surface normal of the target (the 45-degree crossing angle toward the XFEL beam) and probes the area irradiated by the XFEL beam. The target images are captured by a long working distance microscope and a charge-coupled-device (CCD) camera (OPAL-2000, Adimec, Eindhoven, The Netherlands). Figure 15a indicates the camera image of the timing monitor and the projection trace of the area irradiated by the XFEL beam. The precipitous edge in the projection trace was formed by the pulse front of the XFEL beam. The spatial decoding

method can convert the edge position to the relative arrival time of the XFEL pulse to the optical laser pulse. The coefficient for the conversion is calibrated as 2.478 fs/pixel by scanning the linear stage delay line. We measured a long-term shift of the relative timing using the timing monitor. Figure 15b,c show a histogram of 3000 shots and trends of averages and standard deviations in 3000 shots in 24 h, respectively. The timing fluctuations have been reduced down to 50 fs (rms) by the synchronization system using BOMPD. However, there still remains a long-term drift of ~0.5 ps in a day. This drift can be suppressed by controlling an RF phase of the mode-locked oscillator using the 'out-of-loop' BOMPD output, which has a linear correlation with the timing monitor.

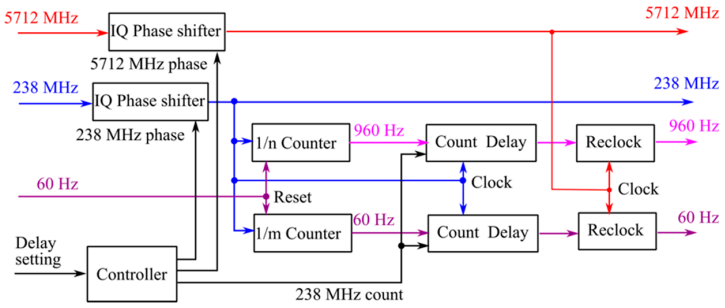

Figure 13. Block diagram of the timing delay unit (TDU). The TDU consists of counters and in-phase and quadrature (IQ) phase shifters. The input signals of 5712 MHz, 238 MHz, and 60 Hz are provided from the SACLA accelerator. The 960-Hz and 60-Hz signals required for the laser operation are produced by counting 238-MHz RF and re-clocking with 5.7-GHz RF. The synchronization to the electron bunch is realized by resetting the count of RF with the 60-Hz timing signal reflecting the timing of the electron bunch. The TDU can delay the output signals of 5712 MHz, 238 MHz, 960 Hz, and 60 Hz simultaneously by setting the parameters of the 5712-MHz RF phase, 238-MHz RF phase, and 238-MHz count delays calculated from the input delay value. The delay value can be set in the range from −2 to +990 microsecond (positive: the XFEL pulses arrives after the optical laser pulses, negative: opposite) with sub-picosecond accuracy.

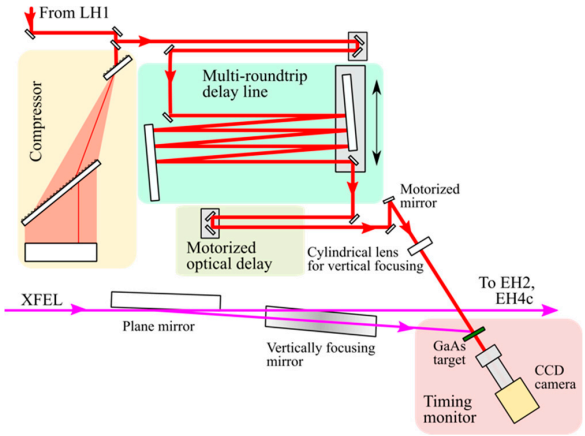

Figure 14. Optical setup for the timing monitor at EH1. The optical laser beam, which is split from the main beam before the seven-pass amplifier, is transported to EH1 and compressed by the pair of transmission gratings. The optical stage delay line and the 1-m long multi-roundtrip delay line are set up to adjust the optical path length, which should be matched with that to the sample position at EH2 or EH4c. About 10% of the XFEL beam split by the transmit grating is vertically focused on the GaAs target in the timing monitor by the elliptical mirror. The GaAs target is mounted with the incidence angle of 45 degrees toward the XFEL beam for spatial decoding. The optical laser beam probes the area irradiated by the XFEL beam with a direction of the surface normal of the target. The target images are captured by the long working distance microscope and the charge-coupled device (CCD) camera.

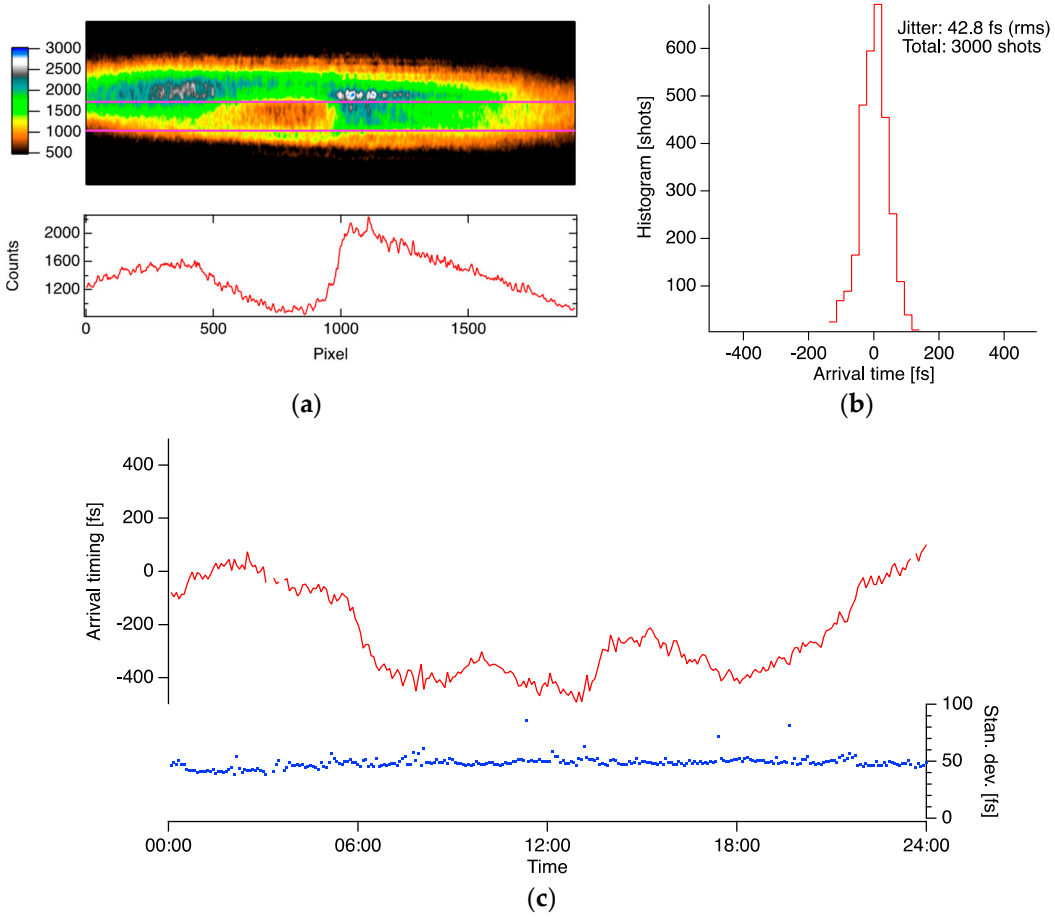

Figure 15. (**a**) Camera image of the timing monitor and vertical projection trace in the irradiated area by the XFEL (indicated by pink lines); (**b**,**c**) statistical data of the relative arrival timing between the XFEL and the optical laser pulses; (**b**) histogram of 300 shots; (**c**) trends of averages (red) and standard deviations (blue) in 24 h.

4. Time-Resolved X-ray Diffraction Measurement

As a demonstration, we performed time-resolved X-ray diffraction (tr-XRD) measurement of photo-excited bismuth (Bi), which has been used as a standard sample for evaluation of pump-probe measurements using XFEL and femtosecond optical laser [6], at EH2. The schematic of the experimental setup is illustrated in Figure 2. A Bi thin film with a 53-nm thickness on Si (111) substrate was mounted on a diffractometer (5042, HUBER Diffraktionstechnik GmbH & Co. KG, Rimsting, Germany) with a Bragg angle of Bi (111) (~9 degrees). The monochromatized XFEL beam at 10 keV was focused on the Bi sample by compound refractive lenses to the spot size of ~100 µm in diameter (FWHM) [37]. The diffracted signal of Bi (111) was captured by a multi-port CCD (MPCCD) detector [38]. The optical laser beam was propagated to the Bi sample with a crossing angle of 3 degrees toward the XFEL beam through a prism shape mirror. We focused the optical laser beam to a spot size of about 1 mm in diameter on the sample with a 1-m focal length lens and adjusted the fluence at 1.0 mJ/cm^2 with a variable neutral density filter. The beam spot of the optical laser was matched to that of the XFEL by tuning the motorized mirror and lens holders. The sample condition irradiated by the optical laser and the XFEL beams was observed by long working distance microscopes. The temporal overlap between the XFEL and the optical laser pulses at the sample position was roughly evaluated by monitoring both signals with a fast photodiode (G4176-03, Hamamatsu Photonics K.K., Hamamatsu, Japan) and a high precision oscilloscope (MSOV164A, Keysight Technologies, Santa Rosa, CA, USA) with several tens-of-picosecond accuracies. Finally, we optimized spatiotemporal overlap between the XFEL and the optical laser beams with the diffracted signal from the Bi sample. Figure 16a shows the total

intensity of the diffracted X-rays as a function of delay, which was normalized by the incident XFEL intensity. The red trace indicates raw data of the delay scan with a 33-fs step, while the blue trace shows post-processed data for the jitter error correction with the timing monitor. We observed the coherent phonon excited by the optical laser in Bi even without the post-processing because the optical laser was precisely synchronized using the BOMPD with a jitter of 50 fs. As a comparison, Figure 16b shows the results of the previous experiment with the same setup, which was conducted when the optical laser was synchronized by a commercial locking system using a fast photo-detector with about 0.3-ps jitter (Synchrolock AP, Coherent Inc., Santa Clara, CA, USA). The diffraction signal changes gently as scanning the delay, as shown in the blue trace, while the oscillation appears after the jitter error correction, as shown in the red trace. Note that the fluence of the optical laser was increased up to 2.0 mJ/cm^2 to make a contrast of the oscillation in the previous experiment.

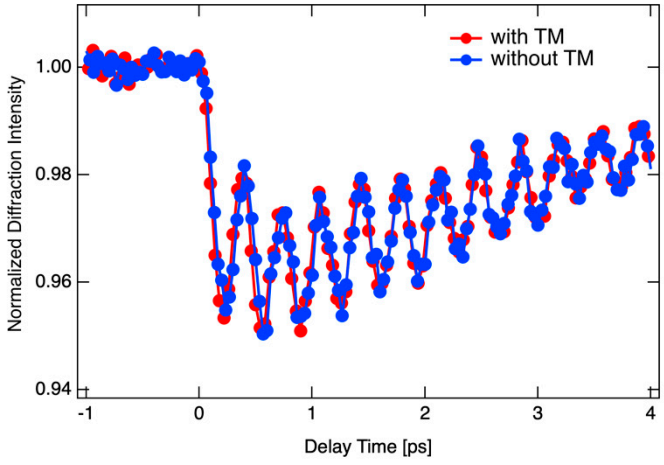

(**a**)

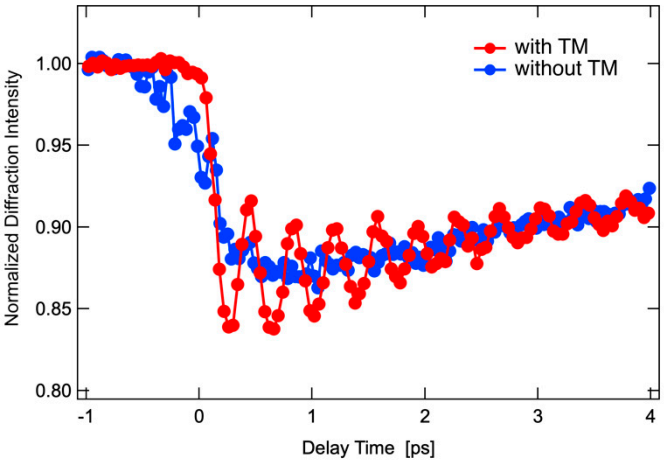

(**b**)

Figure 16. Diffraction intensity of Bi (111) as a function of delay time. The blue and red traces show the raw data obtained by scanning the delay and the data post-processed using the timing monitor. The optical laser was synchronized by the systems using BOMPD (**a**) and a fast photo-detector (**b**). The fluences of the optical laser were 1.0 and 2.0 mJ/cm^2 in (**a**) and (**b**), respectively.

5. Conclusions

We constructed the femtosecond optical laser system based on Ti:sapphire chirped-pulse amplifier with spatiotemporal stabilization for pump-probe experiments at SACLA. Stabilization of output power and pointing has been achieved with a fluctuation level of a few percent by controlling the condition of temperature and air-flow in the optical paths. We optimized the shapes of the fundamental

pulses with durations of ~40 fs by monitoring SPIDER and evaluated the SH and TH pulses with FROG. The new feedback system using BOMPD has successfully reduced the jitter down to 50 fs. We demonstrated the temporal stability with the tr-XRD measurement and successfully observed the coherent phonon oscillation of the photo-excited Bi without the post-processing with the timing monitor. This laser system is expected to realize high precision experiments of time-resolved X-ray absorption and emission spectroscopy, X-ray diffraction, and X-ray scattering for studying ultrafast dynamics.

Author Contributions: Design and development of the optical laser system, T.T. and S.O.; Development of synchronization and timing systems of the optical laser, T.T., K.S., and H.T.; Development of the timing monitor and the XFEL optics, T.K., S.O., and T.T.; Development of the XFEL beamlines and experimental apparatuses, K.T., T.K., Y.U., T.T., T.Y., and M.Y.; Time-resolved X-ray diffraction experiment and analysis, Y.K. and T.T.; Data analysis and visualization, T.T.; Writing—original draft preparation, T.T.; Writing—review and editing, T.Y. and M.Y.; Project administration, M.Y. All authors have read and agreed to the published version of the manuscript.

Funding: This research received no external funding.

Acknowledgments: The authors are grateful to Suguru Ito (Department of Physics, Philipps-University of Marburg, Marburg, Germany) and Iwao Matsuda (Institute for Solid State Physics, The University of Tokyo, Kashiwa, Chiba, Japan) for the production of the Bi thin-film sample. The authors also acknowledge all the SACLA staff for their support.

Conflicts of Interest: The authors declare no conflict of interest.

References

1. McNeil, B.W.J.; Thompson, N.R. X-ray free-electron lasers. *Nat. Photonics* **2010**, *4*, 814–821. [CrossRef]
2. Emma, P.; Akre, R.; Arthur, J.; Bionta, R.; Bostedt, C.; Bozek, J.; Brachmann, A.; Bucksbaum, P.; Coffee, R.; Decker, F.-J.; et al. First lasing and operation of an ångstrom-wavelength free-electron laser. *Nat. Photonics* **2010**, *4*, 641–647. [CrossRef]
3. SLAC National Accelerator Laboratory. Linac Coherent Light Source II Conceptual Design Report, No. SLAC-R-978. Available online: https://www.osti.gov/biblio/1029479-linac-coherent-light-source-ii-lcls-ii-conceptual-design-report (accessed on 8 November 2020). [CrossRef]
4. Tschentscher, T.; Bressler, C.; Grünert, J.; Madsen, A.; Mancuso, P.; Meyer, M.; Scherz, A.; Sinn, H.; Zastrau, U. Photon Beam Transport and Scientific Instruments at the European XFEL. *Appl. Sci.* **2017**, *7*, 592. [CrossRef]
5. Ishikawa, T.; Aoyagi, H.; Asaka, T.; Asano, Y.; Azumi, N.; Bizen, T.; Ego, H.; Fukami, K.; Fukui, T.; Furukawa, Y.; et al. A compact X-ray free-electron laser emitting in the sub-ångstrom region. *Nat. Photonics* **2012**, *6*, 540–544. [CrossRef]
6. Kang, S.K.; Min, C.K.; Heo, H.; Kim, C.; Yang, H.; Kim, G.; Nam, I.; Baek, S.Y.; Choi, H.J.; Mun, G.; et al. Hard X-ray free-electron laser with femtosecond—Scale timing jitter. *Nat. Photonics* **2017**, *11*, 708–713. [CrossRef]
7. Milne, C.J.; Schietinger, T.; Aiba, M.; Alarcon, A.; Alex, J.; Anghel, A.; Arsov, V.; Beard, C.; Beaud, P.; Bettoni, S.; et al. SwissFEL: The Swiss X-ray Free Electron Laser. *Appl. Sci.* **2017**, *7*, 720. [CrossRef]
8. Kim, K.H.; Kim, J.G.; Nozawa, S.; Sato, T.; Oang, K.Y.; Kim, T.W.; Ki, H.; Jo, J.; Park, S.; Song, C.; et al. Direct observation of bond formation in solution with femtosecond X-ray scattering. *Nature* **2015**, *518*, 385–389. [CrossRef]
9. Ogi, Y.; Obara, Y.; Katayama, T.; Suzuki, Y.-I.; Liu, S.Y.; Bartlett, N.C.-M.; Kurahashi, N.; Karashima, S.; Togashi, T.; Inubushi, Y.; et al. Ultraviolet photochemical reaction of $[Fe(III)(C_2O_4)_3]^{3-}$ in aqueous solutions studied by femtosecond time-resolved X-ray absorption spectroscopy using an X-ray free electron laser. *Struct. Dyn.* **2015**, *2*, 034901. [CrossRef]
10. Obara, Y.; Ito, H.; Ito, T.; Kurahashi, N.; Thürmer, S.; Tanaka, H.; Katayama, T.; Togashi, T.; Owada, S.; Yamamoto, Y.; et al. Femtosecond time-resolved X-ray absorption spectroscopy of anatase TiO_2 nanoparticles using XFEL. *Struct. Dyn.* **2017**, *4*, 044033. [CrossRef]
11. Kim, J.G.; Nozawa, S.; Kim, H.; Choi, E.H.; Sato, T.; Kim, T.W.; Kim, K.H.; Ki, H.; Kim, J.; Choi, M.; et al. Mapping the emergence of molecular vibrations mediating bond formation. *Nature* **2020**, *582*, 520–524. [CrossRef]

12. Kinschel, D.; Bacellar, C.; Cannelli, O.; Sorokin, B.; Katayama, T.; Mancini, G.F.; Rouxel, J.R.; Obara, Y.; Nishitani, J.; Ito, H.; et al. Femtosecond X-ray emission study of the spin cross-over dynamics in haem proteins. *Nat. Commun.* **2020**, *11*, 4145. [CrossRef] [PubMed]
13. Katayama, T.; Northey, T.; Gawelda, W.; Milne, C.J.; Vankó, G.; Lima, F.; Bohinc, R.; Németh, Z.; Nozawa, S.; Sato, T.; et al. Tracking multiple components of a nuclear wavepacket in photoexcited Cu(I)-phenanthroline complex using ultrafast X-ray spectroscopy. *Nat. Commun.* **2019**, *10*, 3606. [CrossRef] [PubMed]
14. Dean, M.P.M.; Cao, Y.; Liu, X.; Wall, S.; Zhu, D.; Mankowsky, R.; Thampy, V.; Chen, X.M.; Vale, J.G.; Casa, D.; et al. Ultrafast energy- and momentum-resolved dynamics of magnetic correlations in the photo-doped Mott insulator Sr_2IrO_4. *Nat. Mater.* **2016**, *15*, 601. [CrossRef] [PubMed]
15. Kubli, M.; Savoini, M.; Abreu, E.; Burganov, B.; Lantz, G.; Huber, L.; Neugebauer, M.J.; Boie, L.; Esposito, V.; Bothschafter, E.M.; et al. Kinetics of a Phonon-Mediated Laser-Driven Structural Phase Transition in $Sn_2P_2Se_6$. *Appl. Sci.* **2019**, *9*, 525. [CrossRef]
16. Esposito, V.; Rettig, L.; Bothschafter, E.M.; Deng, Y.; Dornes, C.; Huber, L.; Huber, T.; Ingold, G.; Inubushi, Y.; Katayama, T.; et al. Dynamics of the photoinduced insulator-to-metal transition in a nickelate film. *Struct. Dyn.* **2018**, *5*, 064501. [CrossRef] [PubMed]
17. Trigo, M.; Giraldo-Gallo, P.; Kozina, M.E.; Henighan, T.; Jiang, M.P.; Liu, H.; Clark, J.N.; Chollet, M.; Glownia, J.M.; Zhu, D.; et al. Coherent order parameter dynamics in $SmTe_3$. *Phys. Rev. B* **2019**, *99*, 104111. [CrossRef]
18. Yamamoto, K.; Kubota, Y.; Suzuki, M.; Hirata, Y.; Carva, K.; Berritta, M.; Takubo, K.; Uemura, Y.; Fukaya, R.; Tanaka, K.; et al. Ultrafast demagnetization of Pt magnetic moment in L10-FePt probed by magnetic circular dichroism at a hard X-ray free electron laser. *N. J. Phys.* **2019**, *21*, 123010. [CrossRef]
19. Pergament, M.; Palmer, G.; Kellert, M.; Kruse, K.; Wang, J.; Wissmann, L.; Wegner, U.; Emons, M.; Kane, D.; Priebe, G.; et al. Versatile optical laser system for experiments at the European X-ray free-electron laser facility. *Opt. Exp.* **2016**, *24*, 29349. [CrossRef] [PubMed]
20. Palmer, G.; Kellert, M.; Wang, J.; Emons, M.; Wegner, U.; Kane, D.; Pallas, F.; Jezynski, T.; Venkatesan, S.; Rompotis, D.; et al. Pump-probe laser system at the FXE and SPB/SFX instruments of the European X-ray Free-Electron Laser Facility. *J. Synchrotron Rad.* **2019**, *26*, 328. [CrossRef] [PubMed]
21. Mecseki, K.; Windeler, M.K.R.; Miahnahri, A.; Robinson, J.S.; Fraser, J.M.; Fry, A.R.; Tavella, F. High average power 88 W OPCPA system for high-repetition-rate experiments at the LCLS x-ray free-electron laser. *Opt. Lett.* **2019**, *44*, 1257–1260. [CrossRef] [PubMed]
22. Windeler, M.K.R.; Mecseki, K.; Miahnahri, A.; Robinson, J.S.; Fraser, J.M.; Fry, A.R.; Tavella, F. 100 W high-repetition-rate near-infrared optical parametric chirped pulse amplifier. *Opt. Lett.* **2019**, *44*, 4287–4290. [CrossRef]
23. Sato, T.; Togashi, T.; Ogawa, K.; Katayama, T.; Inubushi, Y.; Tono, K.; Yabashi, M. Highly efficient arrival timing diagnostics for femtosecond X-ray and optical laser pulses. *Appl. Phys. Exp.* **2015**, *8*, 012702. [CrossRef]
24. Katayama, T.; Owada, S.; Togashi, T.; Ogawa, K.; Karvinen, P.; Vartiainen, I.; Eronen, A.; David, C.; Sato, T.; Nakajima, K.; et al. A beam branching method for timing and spectral characterization of hard X-ray free-electron lasers. *Struct. Dyn.* **2016**, *3*, 034301. [CrossRef] [PubMed]
25. Nakajima, K.; Joti, Y.; Katayama, T.; Owada, S.; Togashi, T.; Abe, T.; Kameshima, T.; Okada, K.; Sugimoto, T.; Yamaga, M.; et al. Software for the data analysis of the arrival-timing monitor at SACLA. *J. Synchrotron Rad.* **2018**, *25*, 592–603. [CrossRef] [PubMed]
26. Tono, T.; Togashi, T.; Inubushi, Y.; Sato, T.; Katayama, T.; Ogawa, K.; Ohashi, H.; Kimura, H.; Takahashi, S.; Takeshita, K.; et al. Beamline, experimental stations and photon beam diagnostics for the hard X-ray free electron laser of SACLA. *N. J. Phys.* **2013**, 15083035. [CrossRef]
27. Strickland, D.; Mourou, G. Compression of amplified chirped optical pulses. *Opt. Commun.* **1985**, *56*, 219–221. [CrossRef]
28. Verluise, F.; Laude, V.; Cheng, Z.; Spielmann, C.; Tournois, P. Amplitude and phase control of ultrashort pulses by use of an acousto-optic programmable dispersive filter: Pulse compression and shaping. *Opt. Lett.* **2000**, *25*, 575. [CrossRef]
29. Iaconis, C.; Walmsley, I.A. Spectral phase interferometry for direct electric-field reconstruction of ultrashort optical pulses. *Opt. Lett.* **1998**, *23*, 792. [CrossRef] [PubMed]

30. Trebino, R. *Frequency-Resolved Optical Gating: The Measurement of Ultrashort Laser Pulses*; Springer: Berlin/Heidelberg, Germany, 2000.
31. Kim, J.; Kärtner, F.X.; Perrott, M.H. Femtosecond synchronization of radio frequency signals with optical pulse trains. *Opt. Lett.* **2004**, *29*, 2076. [CrossRef] [PubMed]
32. Jung, K.; Kim, J. Subfemtosecond synchronization of microwave oscillators with mode-locked Er-fiber lasers. *Opt. Lett.* **2012**, *37*, 2958. [CrossRef]
33. Peng, M.Y.; Kalaydzhyan, A.; Kärtner, F.X. Balanced optical-microwave phase detector for sub-femtosecond optical-RF synchronization. *Opt. Express* **2014**, *22*, 27102. [CrossRef] [PubMed]
34. Fukuyama, Y.; Yasuda, N.; Kim, J.; Murayama, H.; Ohshima, T.; Tanaka, Y.; Kimura, S.; Kamioka, H.; Moritomo, Y.; Toriumi, K.; et al. Ultra-high-precision time control system over any long time delay for laser pump and synchrotron x-ray probe experiment. *Rev. Sci. Instrum.* **2008**, *79*, 045107. [CrossRef]
35. Owada, S.; Nakajima, K.; Togashi, T.; Kayatama, T.; Yabashi, M. Single-shot arrival timing diagnostics for a soft X-ray free-electron laser beamline at SACLA. *J. Synchrotron Rad.* **2018**, *25*, 68–71. [CrossRef] [PubMed]
36. Owada, S.; Nakajima, K.; Togashi, T.; Katayama, T.; Yumoto, H.; Ohashi, H.; Yabashi, M. Arrival timing diagnostics at a soft X-ray free-electron laser beamline of SACLA BL1. *J. Synchrotron Rad.* **2019**, *26*, 887–890. [CrossRef]
37. Katayama, T.; Hirano, T.; Morioka, Y.; Sano, Y.; Osaka, T.; Owada, S.; Togashi, T.; Yabashi, M. X-ray optics for advanced pump-probe X-ray experiments at SACLA. *J. Synchrotron Rad.* **2019**, *26*, 333–338. [CrossRef] [PubMed]
38. Kameshima, T.; Ono, S.; Kudo, T.; Ozaki, K.; Kirihara, Y.; Kobayashi, K.; Inubushi, Y.; Yabashi, M.; Horigome, T.; Holland, A.; et al. Development of an X-ray pixel detector with multi-port charge-coupled device for X-ray free-electron laser experiments. *Rev. Sci. Instrum.* **2014**, *85*, 033110. [CrossRef] [PubMed]